

Spectroscopy of low–spin states in ^{157}Dy : Search for evidence of enhanced octupole correlations

S. N. T. Majola^{1,2,3*}, R. A. Bark³, L. Bianco¹², T. D. Bucher³, S. P. Bvumbi², D. M. Cullen^{4,7}, P. E. Garrett¹², P. T. Greenlees⁴, D. Hartley⁸, J. Hirvonen⁴, U. Jakobsson⁴, P. M. Jones³, R. Julin⁴, S. Juutinen⁴, S. Ketelhut⁴, B. V. Kheswa^{2,3}, A. Korichi¹³, E. A. Lawrie^{3,5}, P. L. Masiteng², B. Maqabuka³, L. Mdletshe^{1,3}, A. Minkova¹⁴, J. Ndayishimye³, P. Nieminen⁴, R. Newman³, B. M. Nyakó⁹, S. S. Ntshangase¹, P. Peura⁴, P. Rahkila⁴, L. L. Riedinger¹⁰, M. Riley⁶, D. Roux¹¹, P. Ruotsalainen⁴, J. Saren⁴, J. F. Sharpey-Schafer⁵, C. Scholey⁴, O. Shirinda³, A. Sithole^{1,5}, J. Sorri^{4†}, S. Stolze^{4‡}, J. Timár⁹, J. Uusitalo⁴ and G. Zimba².

¹ University of Zululand, Department of Physics and Engineering, kwaDlangezwa, 3886, South Africa

² Department of Physics, University of Johannesburg, P.O. Box 524, Auckland Park 2006, South Africa

³ iThemba LABS, P. O. Box 722, Somerset–West 7129, South Africa

⁴ University of Jyväskylä, Department of Physics, P.O. Box 35, FI-40014 University of Jyväskylä, Finland

⁵ University of the Western Cape, Department of Physics, P/B X17, Bellville 7535, South Africa

⁶ Department of Physics, Florida State University, Tallahassee, FL 32306, USA

⁷ Schuster Laboratory, University of Manchester, Manchester M13 9PL, United Kingdom.

⁸ Department of Physics, U.S. Naval Academy, Annapolis, Maryland 21402, USA

⁹ MTA Atomki, P.O. Box 51, H-4001 Debrecen, Hungary

¹⁰ University of Tennessee, Department of Physics and Astronomy, Knoxville, Tennessee 37996, USA

¹¹ Department of Physics, Rhodes University, P.O. Box 74, Grahamstown 6140, South Africa

¹² University of Guelph, Department of Physics, Guelph, Ontario N1G 2W1, Canada

¹³ CSNSM–IN2P3–CNRS, F–91405 Orsay Campus, France

¹⁴ University of Sofia, Faculty of Physics, Sofia 1164, Bulgaria

Present addresses: † Sodankylä Geophysical Observatory, University of Oulu, Tähteläntie 62, FI-99600 Sodankylä

‡ Physics Division, Argonne National Laboratory, Argonne, Illinois 60439, USA

*email address: smajola@uj.ac.za

PACS number: 27.70.+q, 21.10.Re, 23.20.Lv

Low–spin states of ^{157}Dy have been studied using the JUROGAM II array, following the $^{155}\text{Gd}(\alpha, 2n)$ reaction at a beam energy of 25 MeV. The level scheme of ^{157}Dy has been expanded with four new bands. Rotational structures built on the $[523]5/2^-$ and $[402]3/2^+$ neutron orbitals constitute new additions to the level scheme as do many of the inter– and intra–band transitions. This manuscript also reports the observation of cross $I^+ \rightarrow (I-1)^-$ and $I^- \rightarrow (I-1)^+$ E1 dipole transitions inter–linking structures built on the $[523]5/2^-$ (band 5) and $[402]3/2^+$ (band 7) neutron orbitals. These interlacing band structures are interpreted as the bands of parity doublets with simplex quantum number $s = -i$ related to possible octupole correlations.

I. Introduction

Octupole correlations are a manifestation of broken reflection symmetry in the nuclear mean-field. Detailed calculations have been performed to determine the ideal properties of the nuclei which exhibit such a feature. Promising candidates have been studied and octupole correlations have been successfully identified and interpreted using various models [1–34, 88]. The appearance of rotational bands with alternating parity, interconnected by E1 transitions, has been identified as one of the indispensable and common properties of nuclei exhibiting enhanced octupole correlations [1, 10, 16, 35, 36]. The occurrence of large E1 transition probabilities (with collective dipole moments) between the yrast positive- and the negative-parity bands is also expected to create a strong evidence for the presence of octupole deformation, which is generally a combination of an axial quadrupole (Y_{20}) and octupole (Y_{30}) shapes [1, 49, 51].

In even-even nuclei, octupole correlations involving the ground state and the associated low-lying collective bands are commonly attributed to the interaction between energetically close $\Delta j = \Delta l = 3$ orbitals of opposite parity. In the transitional rare-earth region, the $f_{7/2} - i_{13/2}$ neutron and $h_{11/2} - d_{5/2}$ proton orbitals ($\Delta j = \Delta l = 3$ single-particle nucleons), which interact via octupole coupling, lie close to the Fermi surface for nuclei with $N \approx 88$. Thus one can expect a maximum effect here [1, 37]. As a result, over the years, experimental manifestations of static and dynamic octupole deformations have been predicted and successfully confirmed by numerous studies in this region of the nuclear chart [9, 18, 26–28, 37, 38–62].

The odd-mass nuclei can also be a suitable test bed for the presence of octupole deformation at low-spin, particularly if the unpaired valence particle orbiting outside an even-even core occupies an orbit that favors reflection asymmetry. Good examples of reflection asymmetry have been reported for some of the odd-mass nuclei in the $N \approx 90$ region, namely the $N=91$ isotones ^{153}Sm and ^{155}Gd [27, 63]. Due to the structural similarities between the $N \approx 90$ isotones in the $A \approx 150$ –160 mass region [64–70], it is reasonable to expect the presence of octupole correlations in ^{157}Dy , which is also an $N = 91$ isotone.

Two previous experiments conducted with large Ge detector arrays used heavy-ion induced reactions $^{150}\text{Nd}(^{12}\text{C},5\text{n})$ and $^{124}\text{Sc}(^{36}\text{S},3\text{n})$ [71, 72, 97] to study the medium to high-spin states of ^{157}Dy . These experiments reported rotational bands built on the $h_{9/2}[521]3/2^-$, $i_{13/2}[651]3/2^+$ and $h_{11/2}[505]11/2^-$ neutrons configurations but reported no transitions linking these structures. To this end we have performed in-beam measurements using the JUROGAM II array to study the rotational bands of ^{157}Dy and to search for evidence of octupole correlations. We report on four new bands as well as many new linking transitions relative to the previously observed structures. The rotational behaviour of the new bands is described in terms of quasi-particle assignments, and the observed alignment properties are analyzed within the framework of the cranked shell model.

II. Experimental details and analysis

Excited states of ^{157}Dy were populated using the $^{155}\text{Gd}(\alpha, 2\text{n})$ reaction at a beam energy of 25 MeV. The ^{155}Gd target was 0.98 mg/cm^2 thick with a purity of 91%. Gamma-rays following the fusion evaporation reaction were detected with the JUROGAM II multi-detector array [73] in JYFL, Jyväskylä, Finland. The spectrometer setup comprised 39 high-purity germanium detectors, all with BGO escape suppression shields; 15 EUROGAM coaxial detectors (Phase I [75] and GASP [74] type) and 24 EUROGAM Phase II clover detectors [76]. Approximately 14×10^9 γ - γ events were unfolded from the data in the off-line analysis and replayed into γ - γ Radware [77, 78] coincidence matrices, which were used to construct the level scheme of ^{157}Dy .

The spins and parities for the new rotational structures were successfully assigned using the Directional Correlation from Oriented States (DCO ratios/ R_{DCO}) [79, 80] and linear polarization anisotropy (A_p) methods [81]. While A_p is given as used in [82], the DCO matrices were constructed using data from detectors in the rings at 158° and $86^\circ+94^\circ$, thus the R_{DCO} for the JUROGAM II array in this work is;

$$R_{DCO} = I_{\gamma_1}(\text{at } 158^\circ : \text{gated on } \gamma_2 \text{ near } 90^\circ) / I_{\gamma_1}(\text{near } 90^\circ : \text{gated on } \gamma_2 \text{ at } 158^\circ) \quad (1)$$

When a gate is set on a known stretched quadrupole transition, a R_{DCO} ratio close to 0.5 and 1.0 is expected for pure stretched dipole and quadrupole transitions, respectively. The electric or magnetic character of transitions was inferred from their A_p values. The A_p values yield $A_p > 0$ and $A_p < 0$ for stretched electric and magnetic transitions, respectively.

III. Experimental results – level scheme

Figures 1 and 2 show partial level schemes of ^{157}Dy deduced in this work. This includes new bands (colored in red) and rotational structures that have been published in previous in-beam works (colored in black). The new Bands 5, 6, 7 and 8 are labeled in the order in which they were discovered. The level scheme presented in this work focuses on the new bands and structures that they feed into – mainly bands built on the $h_{9/2}[521]3/2^-$ and $i_{13/2}[651]3/2^+$ neutron orbitals. Note that the rotational bands associated with the $h_{11/2}[505]11/2^-$ configuration [71, 72] are not shown in Figures 1 and 2 as no new information relevant to the current study was obtained. Measured properties of γ -rays and rotational levels observed in this work are listed in Table 1.

A. Bands 1, 2, 3 and 4

The rotational structures labeled bands 1, 2, 3 and 4 have been previously observed up to high-spins [71, 72, 83]. In this work, bands 1 and 2 are also referred to as the ground band while bands 3 and 4 are sometimes referred to as the yrast band. Apart from R_{DCO} and linear polarization measurements confirming the previous spin and parity assignments (see Table 1), there is no new spectroscopic information reported in this study about these bands. Nevertheless, these bands are important as the majority of the band structures reported for the first time here, decay mainly to them (i.e., bands 1, 2, 3 and 4).

B. Bands 5 and 6

A rotational structure with five in-band transitions, labeled as band 5, has been established in ^{157}Dy . A γ -ray spectrum showing transitions associated with band 5 is shown in Figure 3 (a). This band decays mainly to both signatures of the ground band (i.e. bands 1 and 2) and is built on the rotational level at 341-keV, which was firmly assigned as a $5/2^-$ state by Grotdal *et al.*, [84]. Previously, the level at 527-keV in band 5 was also observed and assigned to be either $5/2^-$ or $7/2^-$ [84, 85]. However, if the $5/2^-$ assignment is considered, the inclusion of the newly discovered 365-keV transition that decays to the $9/2^+$ level in band 3 (see Figure 1) would mean that the 527-keV state would have to decay via a hindered, stretched M2 transition. Similarly, the newly found 229-keV γ -ray, linking the 527-keV level to the $11/2^+$ state of band 4, would also be an M2, if the $7/2^-$ assignment were adopted. Given that an M2 transition is unlikely to compete with the in-band transitions, the possibility of both the $5/2^-$ and $7/2^-$ assignments to the 527-keV level is eliminated, thus leaving a $9/2^-$ assignment. The $9/2^-$ assignment is supported by the R_{DCO} and polarization measurements for the 229 and 466-keV transitions decaying out of the 527-keV level to the $11/2^+$ and $5/2^-$ levels of bands 4 and 1, respectively, see Table 1. For instance, the R_{DCO} for the 229-keV γ -ray is close to 0.5 while that of the 466-keV transition is close to 1. This is consistent with them being stretched dipole and quadrupole transitions, respectively, thus supporting our proposed assignment. The R_{DCO} and polarization measurements performed for other transitions (i.e. 269-, 365- and 379-keV γ -rays) decaying out of the 527-keV level are also consistent with it having a $9/2^-$, see Table 1.

The spin-parity assignments for the remainder of excited levels that form band 5, namely the 827-, 1214-, 1665- and 2154-keV levels have been respectively assigned to $13/2^-$, $17/2^-$, $21/2^-$ and $25/2^-$. These assignments are also supported by the combined results from the DCO and polarization measurements, carried out for the majority of transition decaying out of these levels.

Band 6 is also new, and is composed of six rotational levels, linked by five stretched E2 transitions. A spectrum showing some of the inter-band and intra-band transitions decaying out of Band 6 is shown in Figure 3 (b). Several transitions decaying out of this band feed into the ground (bands 1

and 2) and yrast bands (bands 3 and 4). The multiple decays out of this band and the R_{DCO} and polarization measurements have made it easy to deduce definitive spins and parities for the first three levels of this band; they are $7/2^-$, $11/2^-$ and $15/2^-$ for the 420-, 672- and 1021-keV levels, respectively. The R_{DCO} measurements for the 586-, 783- and 433-keV transitions, which respectively depopulate the 1021- and 672-keV levels are around 0.5 while the polarization measurements for these transitions yield positive values. This is consistent with them being stretched E1 transitions, thus confirming the proposed spin and parity. Polarization measurements were also carried out for the 1006- and 1159-keV γ -rays, which respectively decay out of the 1441- and 1905-keV levels. Measurements for the 1006- and 1159-keV γ -rays yield $A_p = 0.04(2)$ and $A_p = 0.11(6)$; this is consistent with them being stretched electric transitions.

The R_{DCO} and A_p values were also obtained for some of the in-band members, where possible, and they are consistent with them being stretched E2 transitions, see Table 1.

C. Bands 7 and 8

A new band, band 7, is based on a level at 235-keV (see Figure 2), which was previously assigned as $3/2^+$ by Grotdal *et al.*, [84]. A gated spectrum showing some of the in-band members of this band is shown in Figure 3 (c). This band is connected to bands 1, 2, 3, 4, 5 and 8 through numerous decay paths, and this has allowed us to determine and confirm the spin and parity assignments for the first four excited states. As a result, the excitation levels at 235-, 435-, 686- and 1025-keV are respectively assigned to have spins and parities of $3/2^+$, $7/2^+$, $11/2^+$ and $15/2^+$. These assignments are corroborated by the combined results of the R_{DCO} and polarization measurements, performed for a number of inter-band transitions, decaying out of this band. Polarization and R_{DCO} measurements have also been performed for all the in-band transitions of this rotational structure, with the exception of the 251-keV γ -ray, and they yield values that are consistent with these transitions being of stretched E2 character, see Table 1. As a result, the excitation levels at 1421-, 1897- and 2393-keV are respectively assigned spins and parities of $19/2^+$, $23/2^+$ and $27/2^+$.

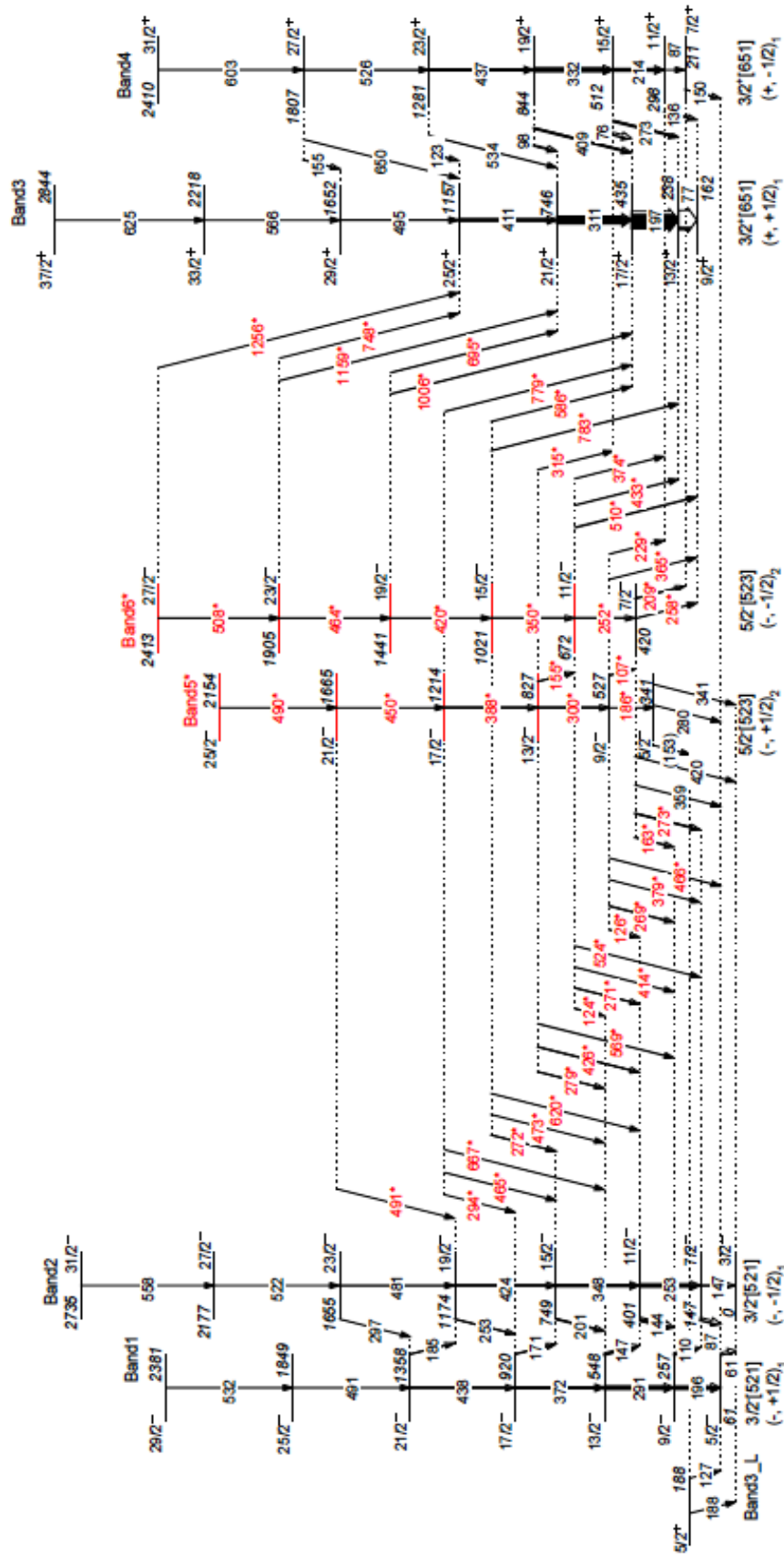


Figure 1: (Color on-line) Partial level scheme of ^{157}Dy deduced from the current work. It shows new rotational structures, bands 5 and 6, which decay predominantly to the ground and yrast bands. New findings from the current work are labeled in red (and marked with asterisk symbols) while previously known bands, deduced from previous in-beam works, are labeled in black. Proposed configurations for each band structure are given below the bands. Quantities within parenthesis are quoted as tentative.

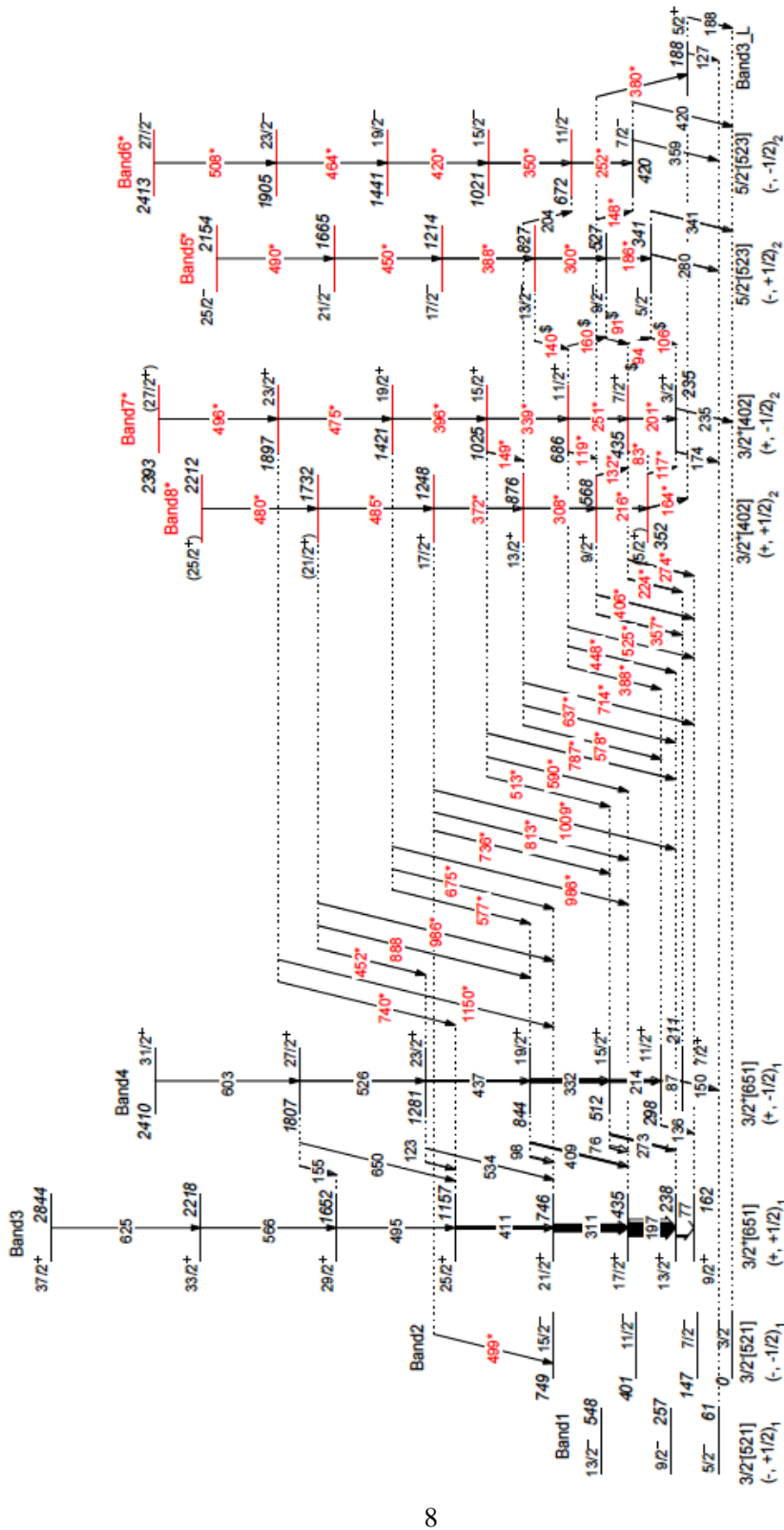


Figure 2: (Color on-line) Partial level scheme of ^{157}Dy deduced from the current work. It shows all the new rotational structures (bands 5, 6, 7 and 8) built on the yrast and ground bands. New findings from the current work are labeled in red (and marked with asterisk symbols) while previously known bands, deduced from previous in-beam works, are labeled in black. Inter-leaving transitions linking bands 5 and 7 are marked with a dollar symbol (\$). Proposed configurations for each band structure are given below the bands. Quantities within parenthesis are quoted as tentative.

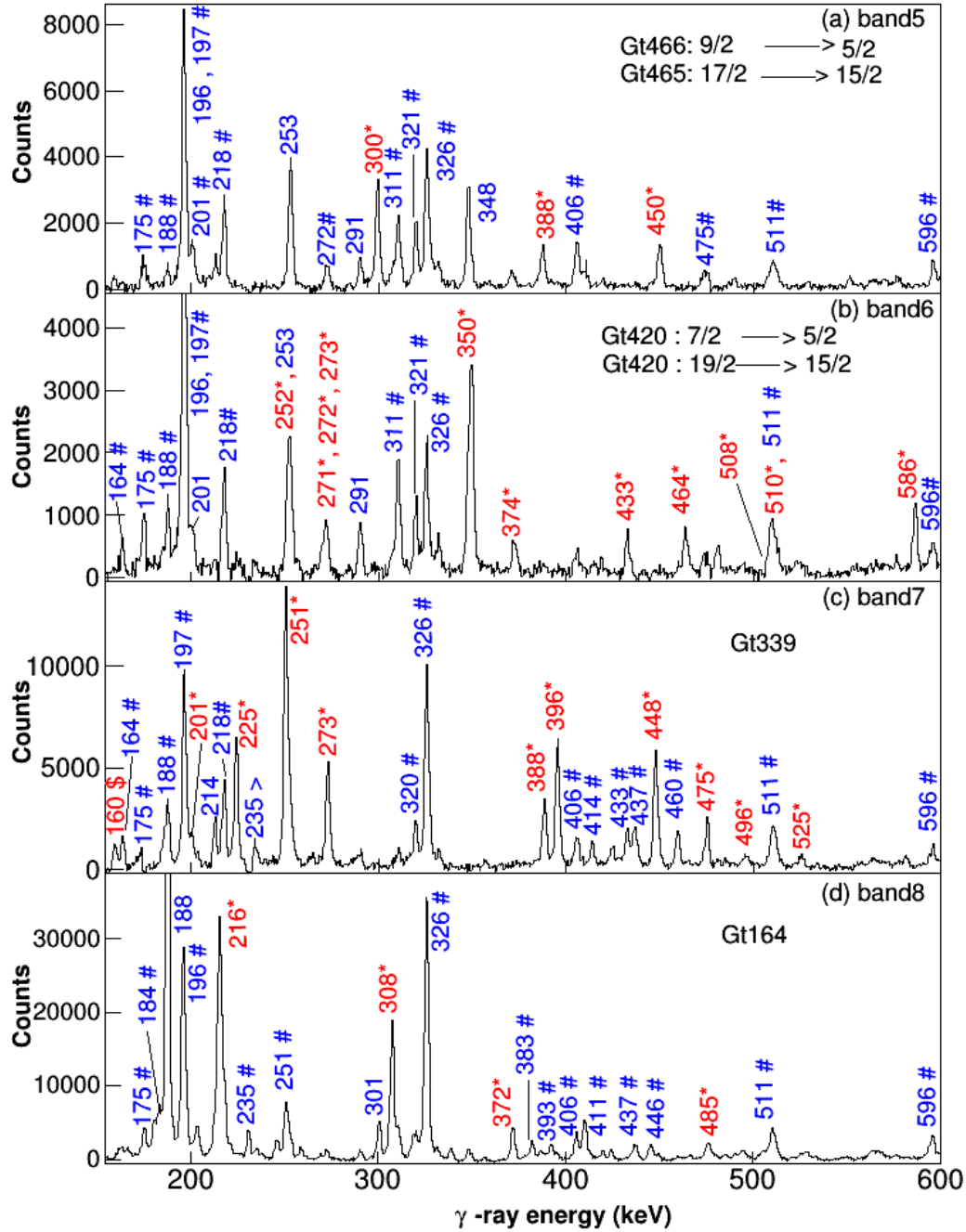


Figure 3 (Color online): Gated coincidence spectra for bands 5, 6, 7 and 8 are shown in panels (a), (b), (c) and (d), respectively. Note that there is an overlap in the single gates set on doublets in (a) and (b). Transitions corresponding to new structures are labeled in red (and marked with asterisk symbols) while contaminant reaction channels and/or other bands of ^{157}Dy , not associated with the cascade of interest are denoted by a colored in blue and marked with hash (#) symbols. The transition marked with a dollar symbol (\$) in Figure 3 (c) is associated with interleaving E1 transition connecting bands 5 and 7. Previously known transitions in the nucleus and/or decay path of interest are also highlighted in blue but are unmarked.

Band 8 is a new rotational sequence built on the 352-keV level. This structure decays mainly to the yrast band with a few transitions going to bands 6 and 7. Numerous γ -rays decaying into and out of band 8, fix the spin and parity assignment of the 568- and 876-keV levels to $9/2^+$ and $13/2^+$, respectively. The R_{DCO} and polarization measurements performed for the 380-keV transition linking the 568-keV state to the 188-keV level in band 3_L (an extension of band3) are consistent with it being a stretched electric transition, thus confirming the proposed spin and parity assignment for the 568-keV level. When taking the proposed assignment for the 568-keV level (i.e., $9/2^+$) into account, the spin-parity assignments for the 352-keV level are restricted to $5/2^+$ or $7/2^+$. Assuming that the 352-, 568- and 876-keV levels are members of band 8, connected to each other via stretched E2 transitions leaves the $5/2^+$ as the only possible spin and parity assignment for the 352-keV level. Indeed, the polarization measurement for the 164-keV transition, linking the state in question to the $5/2^+$ level in band 3_L is $A_p = +0.04(1)$ and is consistent with the 164-keV transition being an unstretched M1 transition. The rest of the levels on this band are placed with the assumption that they are band members connected by stretched E2 transitions.

IV. Discussion

As mentioned above, according to previous studies [71, 72, 83] bands 1 and 2 are built on the ground state of ^{157}Dy , which have been assigned to the $h_{9/2}[521]3/2^-$ neutron configuration. The configuration of bands 3 and 4 ($i_{13/2}[651]3/2^+$) is also known from previous studies [71, 72]. The rotational behaviour of the new bands is described in terms of quasi-particle assignments and the observed alignment properties are analyzed within the framework of the Cranked Shell Model (CSM) [86, 87]. Figure 4 shows a CSM calculation of Routhians e' or quasi-particle energies of ^{157}Dy in a rotating frame, deduced using a modified oscillator potential. The labeling of the quasi-neutron states in Figure 4 is given in Table 2. Configurations proposed for the new bands are also given in this table.

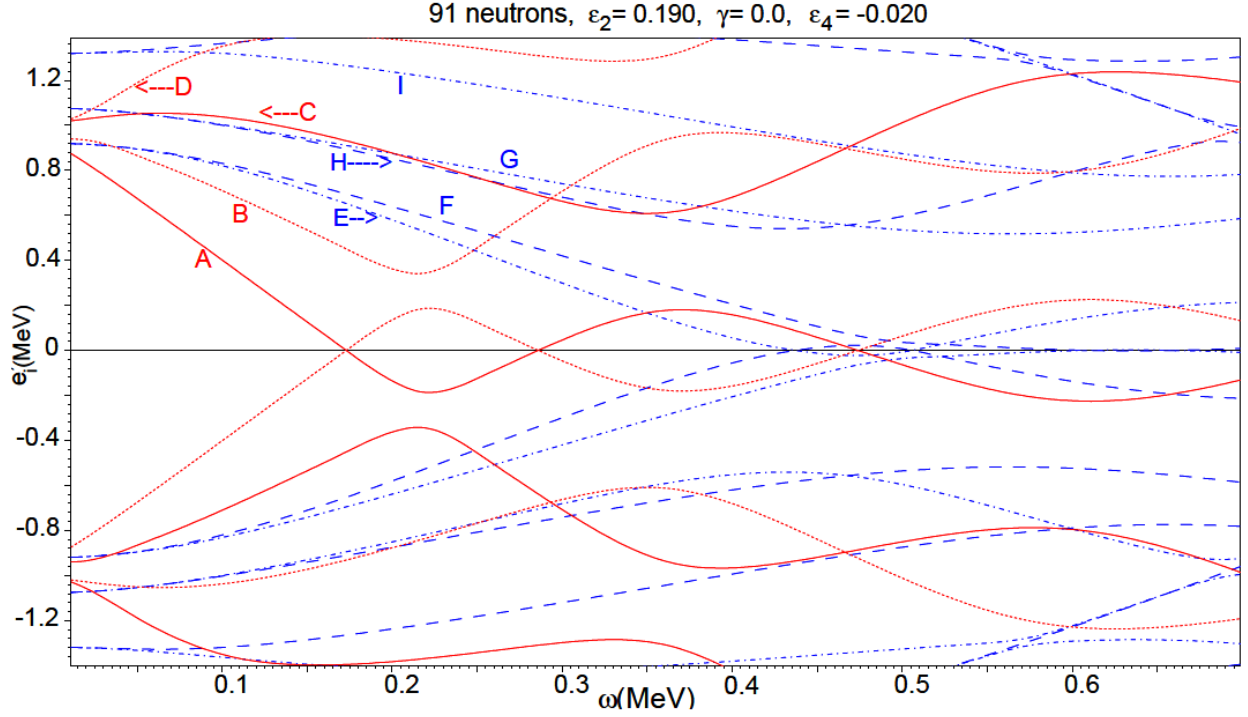


Figure 4: (Color online) Plot of neutron quasi-particle Routhian e_i , as a function of $\hbar\omega$, calculated for ^{157}Dy using the CSM with parameters $\varepsilon_2 = 0.19$, $\varepsilon_4 = -0.020$ and $\gamma = 0^\circ$. The solid and dotted lines colored in red represent positive-parity states with signatures $\alpha = +1/2$ and $-1/2$, respectively. The dot-dashed and dashed lines colored in blue represent negative-parity states with $\alpha = +1/2$ and $-1/2$, respectively. The corresponding quasi-neutron labeling is given in Table 2.

The trajectories presented in this figure correspond to Routhians of orbitals near the Fermi surface, which are most likely to be actively involved in the formation of the band structures observed experimentally in ^{157}Dy . The deformation $\varepsilon_2 = 0.19$, used in the calculation, was found by minimization of the total energy for the $\nu i_{13/2}$ neutron band. This deformation is also appropriate for the $h_{9/2}[521]3/2^-$ and $f_{7/2}[523]5/2^-$ neutron bands, but not for the $d_{3/2}[402]3/2^+$ neutron bands. The optimum minima for these were found to be near $\varepsilon_2 = 0.25$. Therefore the Routhian trajectory for the latter are not visible in Figure 4, as they are too high in energy.

Table 2: Labeling of the quasi–neutron states in figure 4 where $(\pi, \alpha)_n$ represent the n^{th} rotational sequence with signature α and parity π .

<i>band label</i>	$(\pi, \alpha)_n$	Label	Nilsson states
Band1	$(-, +1/2)_1$	E	$h_{9/2}[521]3/2^-$
Band2	$(-, -1/2)_1$	F	$h_{9/2}[521]3/2^-$
Band3	$(+, +1/2)_1$	A	$i_{13/2}[651]3/2^+$
Band4	$(+, -1/2)_1$	B	$i_{13/2}[651]3/2^+$
–	$(+, +1/2)_2$	C	$i_{13/2}[660]1/2^+$
–	$(+, -1/2)_2$	D	$i_{13/2}[660]1/2^+$
Band5	$(-, +1/2)_2$	H	$f_{7/2}[523]5/2^{-*}$
Band6	$(-, -1/2)_2$	G	$f_{7/2}[523]5/2^{-*}$
Band7	$(+, -1/2)_3$	–	$d_{3/2}[402]3/2^{+&}$
Band8	$(+, +1/2)_3$	–	$d_{3/2}[402]3/2^{+&}$

* Strongly mixed with the $h_{9/2}[521]3/2^-$ orbital.

& Strongly mixed with the $i_{13/2}[651]3/2^+$ orbital.

A. Bands 5 and 6

This subsection deals with the quasi–particle excitations responsible for bands 5 and 6. The band head energies of both bands 5 and 6, at 341- and 420-keV, are known from the studies of Grotdal *et al.*, [84] and Klamra *et al.*, [83]. The bands were considered as signature partners associated with the $f_{7/2}[523]5/2^-$ neutron orbital. Indeed, the sequence of levels added in this work, which have allowed us to observe these bands to higher spins, show that these bands share the same moment–of–inertia throughout, as a function of spin, see Figure 5. This feature is also evident in the alignment and Routhian plots, shown in Figures 6 (a) and (b), respectively. In effect, these bands track each other over the observed frequency range. This is consistent with these bands being signature partners built on the same configuration.

In Figure 6 (a), it is apparent that both bands 5 and 6 have an initial alignment close to $1 \hbar$. The modest initial alignment of these bands at low frequencies is a strong indication that an $f_{7/2}$ and/or $h_{9/2}$ orbital is involved in the configuration. The CSM calculations are consistent with bands 5 and 6 being signature partners built on the $f_{7/2}[523]5/2^-$ orbital. Firstly, the alignments predicted for both bands 5 and 6 are $\approx 1.1\hbar$, which matches very well with the value experimentally deduced at $\omega = 0.16$ -MeV (i.e. $\approx 1.2\hbar$), for both bands. According to the quasi-particle Routhian diagram shown in Figure 4, below $\omega = 0.3$ MeV, the slopes corresponding to the $f_{7/2}[523]5/2^-$ configuration (i.e. bands 5 and 6) are predicted to be somewhat parallel to those of structures emanating from the $h_{9/2}[521]3/2^-$ configuration. Indeed, bands 5 and 6 appear to track bands 1 and 2, as predicted in Figure 4. In addition, the relative energy spacing between both structures as well as the order of appearance is also well reproduced, see Figures 4, 5 and 6.

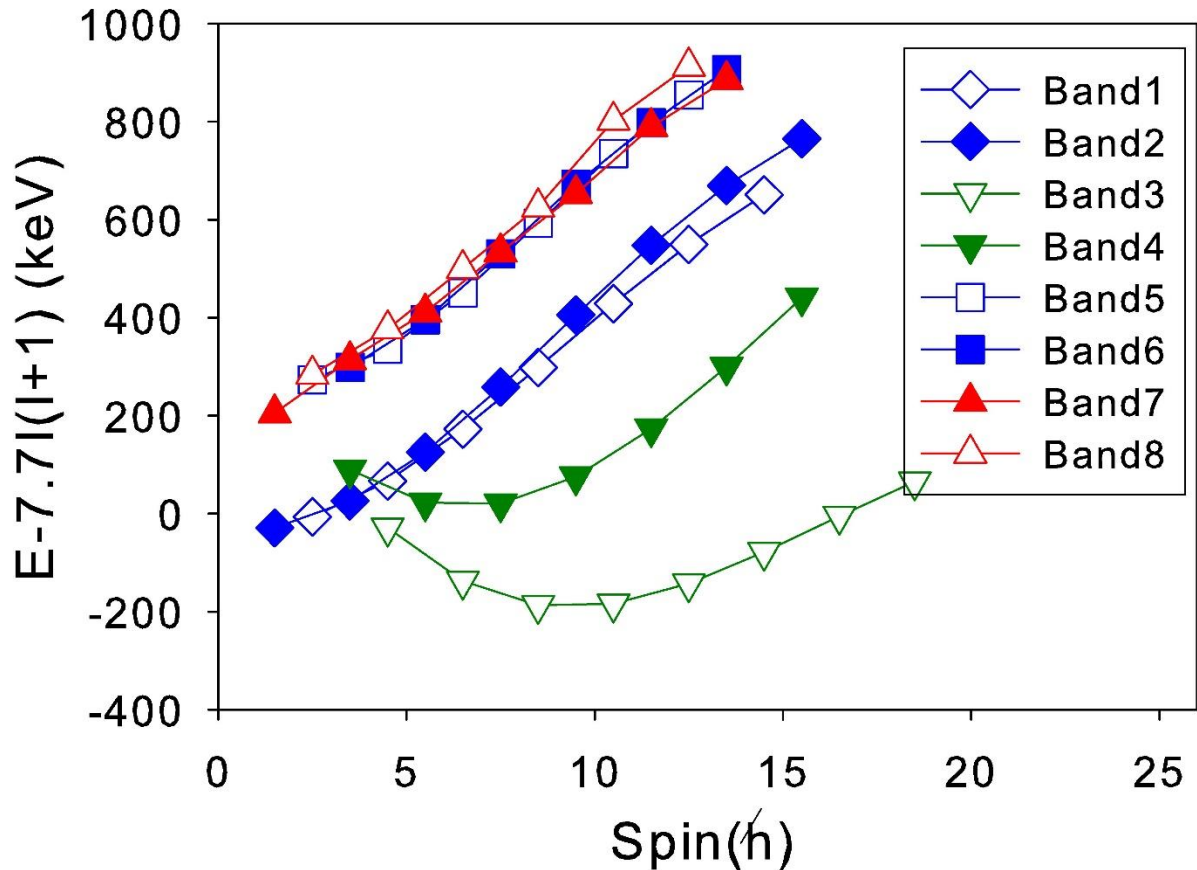


Figure 5: (Color online) Plots of excitation energy minus a rigid rotor reference for the bands observed in ^{157}Dy . Open and closed symbols represent signatures $\alpha = +1/2$ and $\alpha = -1/2$, respectively.

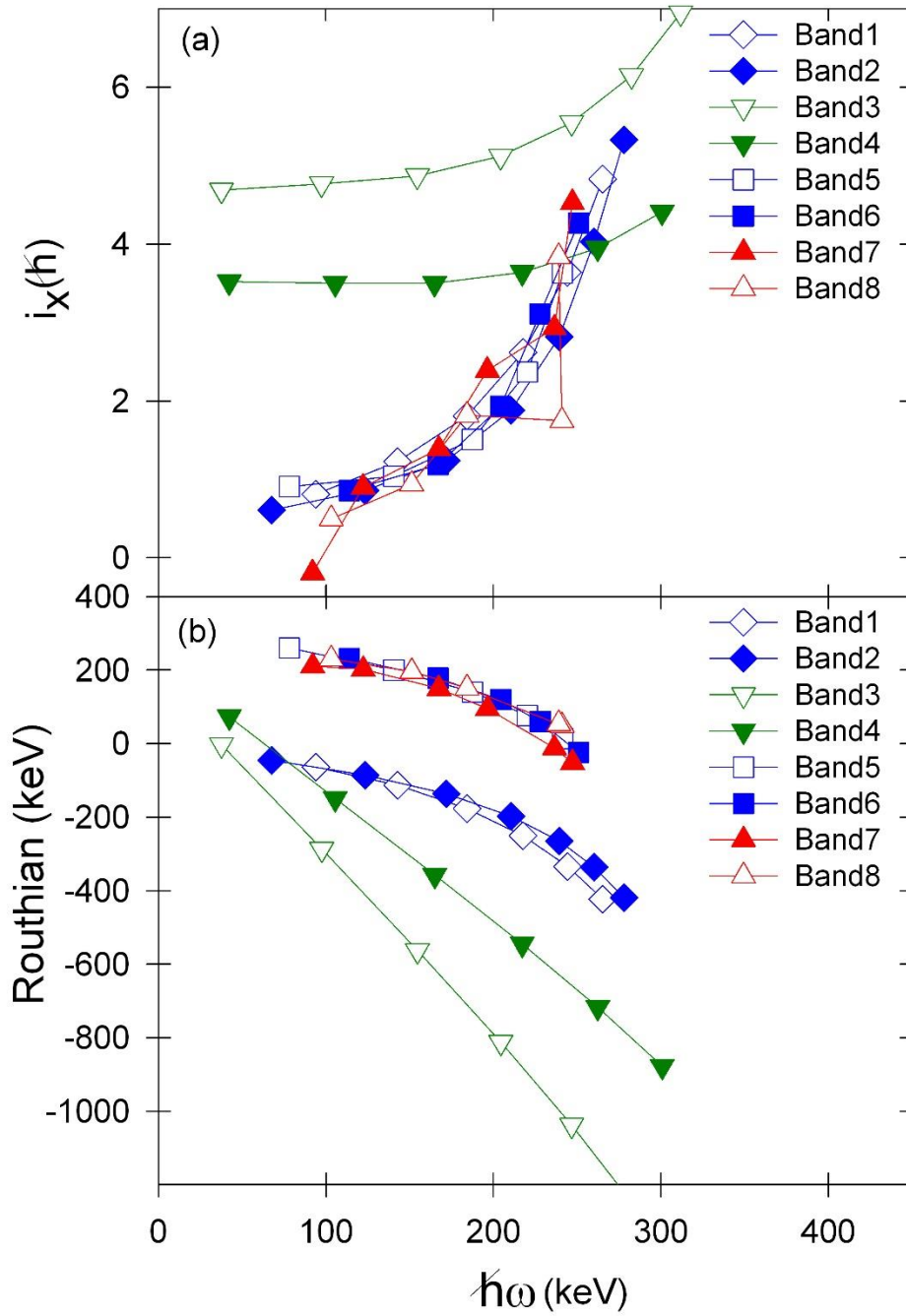


Figure 6: (Color online) Plots of the experimental (a) alignment i_x and (b) Routhians e' for the bands in ^{157}Dy , deduced using Harris parameters of $J_0 = 32 \hbar^2 \text{ MeV}^{-1}$ and $J_1 = 34 \hbar^4 \text{ MeV}^{-3}$. Open and closed symbols represent signatures $\alpha = +1/2$ and $\alpha = -1/2$, respectively.

B. Bands 7 and 8

The interlinking M1 transitions between bands 7 and 8 as well as the manner in which they track one another, both in the alignment and rigid rotor plots, are indicative of them being signature partners. These structures decay mainly to the $i_{13/2}$ bands and are based on a 235-keV level, previously assigned to the $d_{3/2}[402]3/2^+$ neutron configuration [84]. According to [84], this state has admixtures of $i_{13/2}$ neutron orbital, due to the $\Delta N=2$ mixing, caused by the close proximity of the $d_{3/2}[402]3/2^+$ (N=4) and $i_{13/2}[651]3/2^+$ (N=6) Nilsson orbitals at deformation $\epsilon_2 \approx 0.3$. The majority of the positive-parity bands observed in the odd-even nuclei, near the $A \approx 160$ region, are attributed to states associated with the $i_{13/2}$ orbital. In spite of the fact that the bands built on the 235-keV level decay mainly to bands 3 and 4 (the $i_{13/2}$ bands), their structural behavior is somewhat different to that expected for the $i_{13/2}$ bands – in terms of alignment properties, see Figure 6 (a). This is consistent with the fact that the major component of the wave-function of the 235-keV level is dominated by the $d_{3/2}[402]3/2^+$ neutron orbital. Further, the $(+, -1/2)$ signature of the $d_{3/2}[402]3/2^+$ orbital is expected to be the favored one and this is in agreement with what is observed between bands 7 and 8. The apparent upbend observed between $\omega \approx 0.2$ and 0.25 MeV for both bands 7 and 8 in Figure 6 (a) is attributed to the AB crossing following the first alignment of $i_{13/2}$ neutrons [95]. Unlike in the $i_{13/2}$ bands (i.e. bands 3 and 4) where this band crossing is blocked at the cited frequency range, the bands built on $h_{9/2}$ (bands 1 and 2) and $f_{7/2}$ (bands 5 and 6) orbitals are also expected to have similar band crossing frequencies as the $d_{3/2}$ bands (i.e. bands 7 and 8). Indeed, this feature is apparent in the experimental data presented in Figure 6 (a).

C. Possible enhanced octupole correlations in ^{157}Dy

Several pronounced E1 transitions are observed between the bands built on the $f_{7/2}[523]5/2^-$ and $i_{13/2}[651]3/2^+$ configurations (the yrast bands), see Figure 1. The occurrence of relatively large E1 transition probabilities between the yrast positive- and negative-parity bands is one of the indispensable properties of nuclei exhibiting the features of reflection asymmetry [1]. However,

in the odd-mass rare-earth nuclei, more specifically those with $N \approx 91$ such as ^{157}Dy , it is quite common to find a single-particle negative-parity band decaying predominantly to the yrast positive-parity sequence. In a few instances where such a phenomenon has been observed in the $A \approx 160$ mass region, a unique parameter, which accounts for octupole softness has been introduced to help explain this feature [13, 90–93]. The experimental $B(E1)/B(E2)$ ratios of out-of-band to in-band transitions for the γ decays from band 6 have been deduced and are listed in Table 3. The weighted average value of the $B(E1)/B(E2)$ ratios in band 6 is $0.024(1) \times 10^{-6} \text{fm}^{-2}$. This value compares very well with the average weighted values of ratios observed in ^{157}Gd [90], ^{159}Dy [94], ^{161}Er [91], ^{163}Yb [93] and ^{165}Er [92] where evidence of octupole correlations has been manifested through strong E1 transitions. The relatively enhanced $\Gamma^- \rightarrow (I \pm 1)^+$ decays between bands based on these configurations of alternating parity (i.e $[523]5/2^-$ and $[651]3/2^+$ states), could correspond to the $K = 1^-$ octupole degree of freedom in ^{157}Dy . This phenomenon may be attributed to the prevalent octupole coupling of valence nucleons occupying the $\nu(f_{7/2})$ and $\nu(i_{13/2})$ orbitals, which are close to the Fermi-surface and often form the basis for octupole deformation in the $A \approx 150 - 160$ mass region [1]. While these findings might be suggestive that the pronounced $\Gamma^- \rightarrow (I \pm 1)^+$ decays between bands based on the $f_{7/2}[523]5/2^-$ and $i_{13/2}[651]3/2^+$ states, could be due to enhanced octupole correlations, additional experimental quantities, such as $B(E1)s$, would be valuable.

Furthermore, in Figure 2 (and also in Table 1), it is apparent that the rotational sequences of bands 5 and 7 are interlaced with E1 transitions (marked with asterisks in Figure 2), thus forming an alternating parity band. The appearance of rotational bands with alternating parity has been attributed to nuclei having an intrinsic pear shape, which is generated by combining an axial octupole (Y_{30}) with an axial quadrupole (Y_{20}) shape [1]. Rotational states in octupole deformed nuclei are characterized by eigen values s of the simplex operator \mathcal{L} which is related to parity \mathcal{P} and rotation \mathcal{R} operators [23] by:

$$\mathcal{L} = \mathcal{P}\mathcal{R}^{-1} \quad (2)$$

The parity p and spin I of a rotational band with simplex s are related by:

$$p = se^{-i\pi I} \quad (3)$$

Consequently, the resulting simplex quantum number value s of an octupole deformed nuclear system with even (integer I) number of nucleons is restricted to $s = \pm 1$. In an odd- A nucleus such as ^{157}Dy , the possible values of the simplex quantum number are $s = \pm i$, such that [1, 23]:

$$s = -i, \quad I^p = 1/2^-, 3/2^+, 5/2^-, 7/2^+, \dots \quad (4)$$

$$s = +i, \quad I^p = 1/2^+, 3/2^-, 5/2^+, 7/2^-, \dots \quad (5)$$

where $I \geq K$. Therefore, in the current context, according to equation (3) bands 5 and 7 form a reflection asymmetric structure with simplex quantum number $s = -i$.

Nuclei which manifest octupole deformation are expected to have large dipole moments (D_0), thus giving rise to fast E1 transitions, which are expected to compete with intra-band E2 transitions. The experimental $B(E1)/B(E2)$ ratios of the out-of-band to the in-band transitions for the γ decays from the $s = -i$ band have also been deduced in this work and they are listed in Table 3. The weighted average for this ratio is $0.057(28) \times 10^{-6} \text{fm}^{-2}$ for the $s = -i$ candidate in ^{157}Dy . The value is an order of magnitude smaller compared to the $s = -i$ bands of ^{143}Ba and ^{145}Ba [61]. This could imply a modest value for the intrinsic dipole moment. Alternatively, this could also be caused by the larger quadrupole deformation of ^{157}Dy . Indeed, it is known that the prolate deformation of ^{157}Dy is much larger than that of Ba isotopes, which are situated in the island of octupole deformation. In effect, the sudden increase in quadrupole deformation at and beyond $N \approx 90$ may trigger a change in the intrinsic shell structure, which makes the observation of reflection asymmetric shapes rather difficult. In addition, octupole correlations can also be diluted by the intermediate $h_{9/2}$ neutron orbital which comes close to the Fermi level and lies between the $\Delta j = 3$ neutron orbitals – further making it more difficult to confirm the reflection asymmetric configurations [27].

Furthermore, information on the nature of the octupole deformation exhibited by a nucleus can be inferred from the experimental energy displacement $\delta E(I)$, as given by [23]:

$$\delta E(I) = E(I^-) - \frac{1}{2}[E(I+1)^+ + E(I-1)^+] \quad (6)$$

In the case of ^{157}Dy , this is plotted for the $s = -i$ band as shown in Figure 7. Here we compare it to similar structures that have been used to confirm the existence of strong octupole correlations in the rare-earth ($Z \approx 56$, $N \approx 88$) and in the actinide ($Z \approx 90$, $N \approx 134$) regions, namely ^{143}Ba [61] and ^{146}Nd [44]), ^{220}Ra [88] and ^{223}Th [89], respectively.

Clearly, the $s = -i$ structure compares well with simplex structures found in the islands of stable octupole correlations in the ($Z \approx 56$, $N \approx 88$) and ($Z \approx 90$, $N \approx 134$) regions. Furthermore, the energy displacement $\delta E(I)$ is expected to approach 0 for structures exhibiting permanent (or stable) octupole deformation and this feature is evident in the $s = -i$ structure in ^{157}Dy . In effect, this structure is within 5% nearer to $\delta E(I) = 0$ and is the closest to the stable octupole deformation limit (throughout as function of spin I) compared to all other simplex structures shown in Figure 7.

Another approach that can be used to examine the nature of the octupole deformation is through the rotational frequency ratio $\omega^-(I)/\omega^+(I)$ given by [23]:

$$\frac{\omega^-(I)}{\omega^+(I)} = 2 \frac{E(I+1)^- - E(I-1)^-}{E(I+2)^+ - E(I-2)^+} \quad (7)$$

This ratio is expected to approach 1 when nuclei evolve to stable octupole deformation. In order to gain more insight about the octupole correlations in ^{157}Dy , we plot the $\omega^-(I)/\omega^+(I)$ ratio in Figure 8 and compare it to nuclei with octupole enhanced octupole correlations. Here it is clear that the $\omega^-(I)/\omega^+(I)$ ratio for ^{157}Dy is nearer to 1 (within 5% for $I > 5$) whereas it approaches the stable octupole deformation limit at relatively high-spin (spin $I \approx 9$) for simplex structures found

in the well-established octupole nuclei ($Z \approx 56$, $N \approx 88$ and $Z \approx 90$, $N \approx 134$) regions. These results are in accordance with what is expected for a nucleus exhibiting stable octupole deformation.

While the aforementioned bands manifest features that are suggestive of enhanced octupole correlations in ^{157}Dy , it is worth noting that these features cannot be considered as unambiguous proof. It should be noted that there are cases whereby interleaving bands, assigned with the same K-value, could be explained without invoking octupole deformation [2, 17, 20, 96]. Therefore, it is in general, desirable to understand better the features of bands with enhanced octupole correlations. Indeed, additional theoretical and experimental spectroscopic studies (such as lifetime measurements) are thus needed in order to obtain further insight on the existence of enhanced octupole correlation in ^{157}Dy .

Octupole correlations in nuclei are understood to be triggered by the octupole–octupole interaction, which arises between valence nucleons that occupy pairs of orbitals with $\Delta l = 3$ [1, 36]. Band 5 is associated with the $f_{7/2}$ orbital, which mixes strongly with the $h_{9/2}$ orbital. Therefore, if the parity-doublet bands in ^{157}Dy are indeed due to the enhanced octupole correlations, the alternating parity observed between bands 5 and 7 may be attributed to valence nucleons occupying the $h_{9/2}$ and $d_{3/2}$ orbitals, which are likely to be involved in the formation of these bands, such that $\Delta j = 9/2 - 3/2 = 3$.

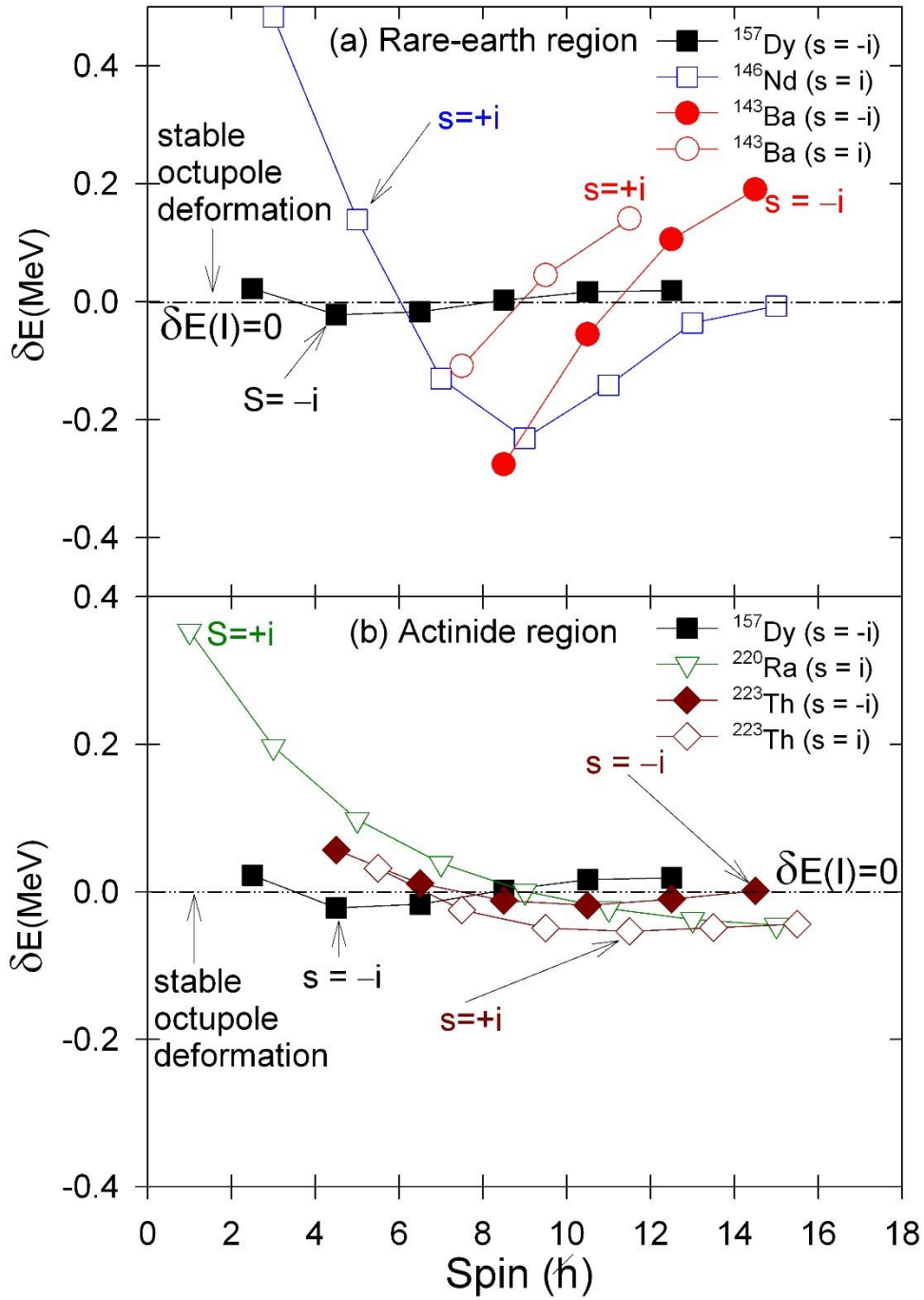


Figure 7: (Color online) Plot of the energy displacement $\delta E(I)$ of bands 5 and 7 forming a reflection asymmetric structure (with simplex $s = -i$) in ^{157}Dy . This structure is compared to similar structures identified in nuclei with considerable octupole deformation in the (a) rare-earth region (^{143}Ba [61] and ^{146}Nd [44]) and (b) actinide region (^{220}Ra [88] and ^{223}Th [89]). The energy displacement $\delta E(I)$ is expected to approach 0 for structures exhibiting permanent octupole deformation. Open and closed symbols correspond to $s = +i$ and $s = -i$ simplex structures, respectively.

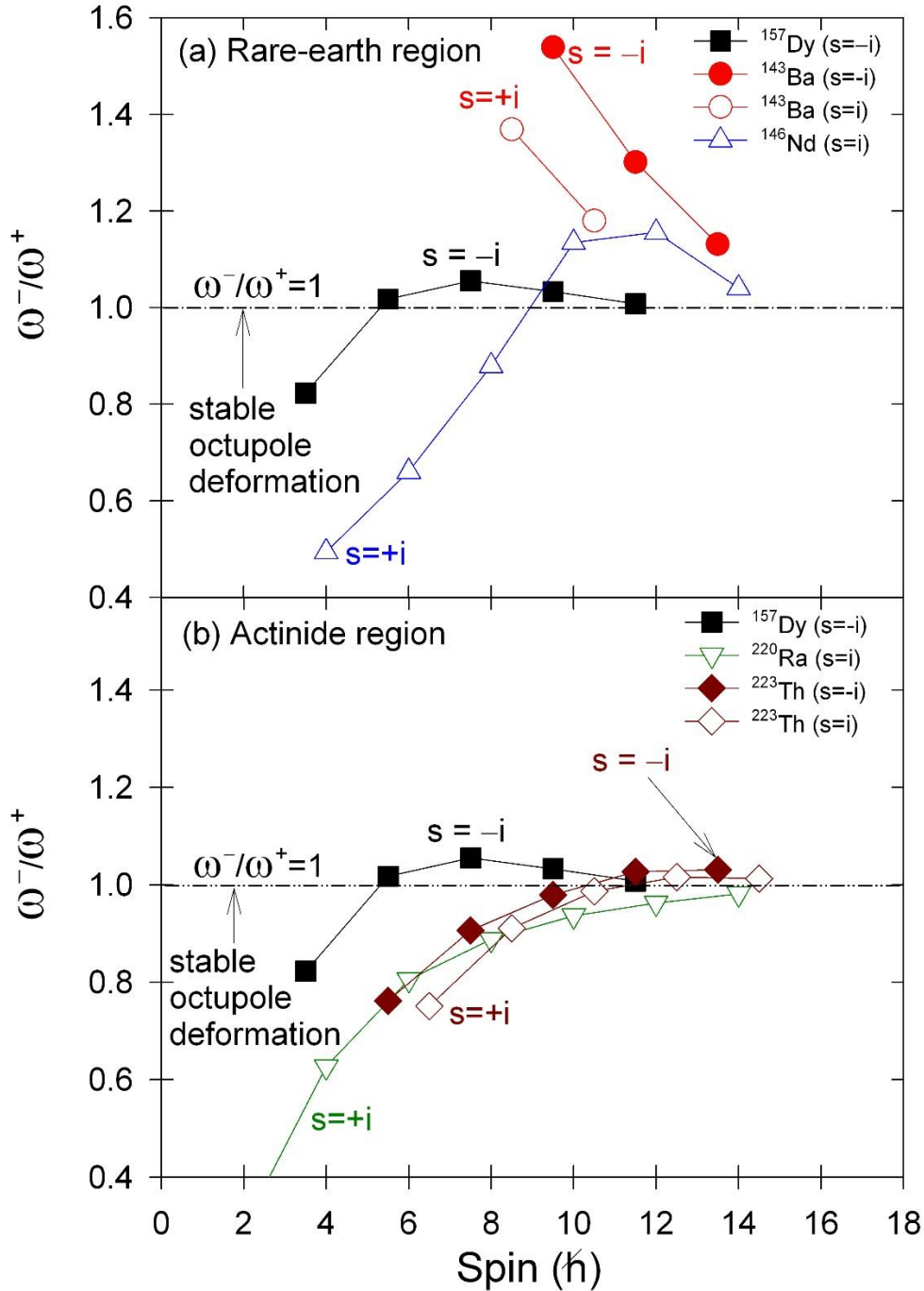


Figure 8: (Color online) Rotational frequency ratio $\omega^-(I)/\omega^+(I)$ of bands 5 and 7 forming a reflection asymmetric structure (with simplex $s = -i$) in ^{157}Dy . This structure is compared to similar structures identified in nuclei with considerable octupole deformation in the (a) rare-earth region (^{143}Ba [61] and ^{146}Nd [44]) and (b) in the actinide region (^{220}Ra [88] and ^{223}Th [89]). This ratio is expected to approach 1 for structures exhibiting stable octupole deformation. Open and closed symbols correspond to $s = +i$ and $s = -i$ simplex structures, respectively.

Table 3: The $B(E1)/B(E2)$ ratios of out-of-band to in-band transitions for the γ decays from the $s = -i$ candidate (band 5 and 7) and band 6 (to the yrast bands) in ^{157}Dy .

$I_i^\pi \rightarrow I_f^\pi$	$E1(\gamma\text{-energy in keV})$	$B(E1)/B(E2), (\times 10^{-6} \text{fm}^{-2})$
$s = -i$		
Bands 5 and 7		
$7/2^+ \rightarrow 5/2^-$	94	0.039(10)
$9/2^- \rightarrow 7/2^+$	91	0.027(3)
$11/2^+ \rightarrow 9/2^-$	160	0.064(8)
$13/2^- \rightarrow 11/2^+$	140	0.096(7)
Band 6		
$11/2^- \rightarrow 9/2^+$	510	0.018(2)
$11/2^- \rightarrow 13/2^+$	433	0.018(1)
$15/2^- \rightarrow 13/2^+$	783	0.007(1)
$15/2^- \rightarrow 17/2^+$	586	0.012(1)
$19/2^- \rightarrow 17/2^+$	1006	0.022(1)
$19/2^- \rightarrow 21/2^+$	695	0.049(2)
$23/2^- \rightarrow 21/2^+$	1159	0.030(2)
$23/2^- \rightarrow 25/2^+$	748	0.042(2)

V. Summary and conclusion

An experiment populating the low-spin states of ^{157}Dy has been performed to investigate the possibility of octupole correlations in this nucleus. The level scheme of ^{157}Dy has been expanded, at low-spin, with four new bands. Bands 5, 6, 7, and 8 constitute new additions to the level scheme of ^{157}Dy , as do many of the intra- and inter-band transitions. Candidates for signature partner bands built on both the $f_{7/2}[523]5/2^-$ and $d_{3/2}[402]3/2^+$ neutron orbitals have been identified for the first time.

This experiment also reports the observation of cross $I^+ \rightarrow (I-1)^-$ and $I^- \rightarrow (I-1)^+$ E1 dipole transitions interlinking structures built on the $[523]5/2^-$ and $[402]3/2^+$ orbitals. The energy displacement $\delta E(I)$ and rotational frequency ratio $\omega^-(I)/\omega^+(I)$ of the resulting parity doublet, formed by interlacing bands 5 and 7, with simplex quantum number $s = -i$ are approximately equal to 0 and 1, respectively. While these bands manifest features that are necessary and essential for a nucleus exhibiting the breaking of the intrinsic reflection symmetry, it is worth noting that they

cannot be considered as unambiguous proof. Therefore, future experimental and theoretical investigative studies are essential in order to positively identify whether the alternating-parity rotational bands, observed in ^{157}Dy , are indeed associated with enhanced octupole correlation.

VI. ACKNOWLEDGEMENTS

This work is supported by the South African National Research Foundation under grants (No. 96829, 109711, 93531, 109134, 116666 and 106012). Support for L.B. and P.E.G. was provided by the Natural Sciences and Engineering Research Council of Canada. JYFL research is supported by the Academy of Finland under the Finnish Centre of Excellence Programme 2006–2011, Contract No. 213503. This work was also partially supported by the National Research, Development and Innovation Fund of Hungary, financed under the K18 funding scheme with project no. K128947, as well as by the European Regional Development Fund (Contract No. GINOP–2.3.3–15–2016–00034). Support for M.R. was provided by the U.S. National Science Foundation under Grant Nos. PHY-1502092 (USNA) and PHY–0754674 (FSU). The authors also acknowledge the support of GAMMAPOOL for the loan of the JUROGAM detectors.

VII. REFERENCES

- [1] P. A. Butler and W. Nazarewicz, *Rev. Mod. Phys.* 68, 349 (1996) and earlier references cited therein.
- [2] R. R. Chasman, *Phys Lett.* B96, 7 (1980).
- [3] R. R. Chasman and I. Ahmad, *Phys. Lett.* B182, 261 (1986).
- [4] S. Cwiok and Nazarewicz, *Phys. Lett.* B224, 5 (1989).
- [5] S. Cwiok and Nazarewicz, *Nucl. Phys.* A496, 367 (1989).
- [6] J.L. Egido and L.M. Robledo, *Nucl. Phys.* A 494, 85 (1989).
- [7] J.L. Egido and L.M. Robledo, *Nucl. Phys.* A 518, 475 (1990).
- [8] J.L. Egido and L.M. Robledo, *Nucl. Phys.* A 524, 65 (1991).
- [9] J.L. Egido and L.M. Robledo, *Nucl. Phys.* A 545, 589 (1992).
- [10] S. Frauendorf *Phys. Rev. C* 77, 021304(R) (2008).
- [11] G. B. Hagemann, I. Hamamoto, and W. Satuła, *Phys. Rev. C* 47, 2008 (1993).
- [12] I. Hamamoto et al., *Phys. Lett.* B 226, 17 (1989).
- [13] I. Hamamoto, *Nucl. Phys.* A 557 (1993) 515c.
- [14] A. Gyurkovich et al., *Phys. Lett.* B 105, 95 (1981).
- [15] Kiuck Lee and D. R. Inglis, *Phys. Rev.* 108, 774 (1957).
- [16] G. A. Leander, R. K. Sheline et al., *Nucl. Phys.* A388, 452 (1982).
- [17] G. A. Leander and R. K. Sheline, *Nucl. Phys.* A413, 375 (1984).
- [18] G.A. Leander et al., *Phys. Lett.* B 152 (1985) 284.
- [19] G. A. Leander and Y. S. Chen, *Phys. Rev.* C35, 1145 (1987).
- [20] G. A. Leander and Y. S. Chen, *Phys. Rev.* C37, 2744 (1988).
- [21] W. Nazarewicz et al., *Nucl. Phys.* A429, 269 (1984).
- [22] W. Nazarewicz et al., *Phys. Rev. Lett.* 52, 1272 (1984).
- [23] W. Nazarewicz and P. Olanders, *Nucl. Phys.* A441, 420 (1985).
- [24] W. Nazarewicz, G. A. Leader, and J. Dudek, *Nucl. Phys.* A467, 437 (1987).
- [25] W. Nazarewicz, *Nucl. Phys.* A520, c333 (1990).
- [26] W. Nazarewicz and S.L. Tabor, *Phys. Rev. C* 45 (1992) 2226.
- [27] D. Nosek, R.K. Sheline, P.C. Sood, and J. Kvasil, *Int. J. Mod. Phys. E*, Vol. 1, 793 (1992).
- [28] D. Nosek et al., *Z. Phys.* A 344, 277 (1993).

- [29] L.M. Robledo et al. J.Phys. G39 (2012) 105103
- [30] I. Ragnarsson, Phys. Lett. B 130, 353 (1983).
- [31] L.M. Robledo, Eur. Phys. J. A (2016)
- [32] L.M. Robledo et al., Phys. Lett. 201B (1988) 409.
- [33] R.K. Sheline et al., Czech J Phys 40, 622 (1990).
- [34] A. Sobiczewski, Z. Patyk, S. Cwiok and P. Rozmej, Nucl. Phys. A485, 16 (1988).
- [35] J. F. C. Cocks et al., Phys. Rev. Lett. 78, 2920 (1997)
- [36] I. Ahmad and P. A. Butler, Annu. Rev. Nucl. Part. Sci. 43, 71 (1993).
- [37] R. H. Spear and W. N. Catford, Phys. Rev. C41, R1351 (1990).
- [38] P. A. Butler and W. Nazarewicz, Nucl. Phys. A 533, 249 (1991).
- [39] S. Bvumbi et al., Phys. Rev. C 87, 044333 (2013).
- [40] S. P. Bvumbi, published PhD thesis, University of the Johannesburg (2014).
- [41] Y. J. Chen et al., Phys. Rev. C 73, 054316 (2006).
- [42] J. H. Hamilton et al., Prog. Part. Nucl. Phys. 35, 635 (1995).
- [43] D.J. Hartley et al., Phys. Rev. C 95, 014321 (2017).
- [44] V. E. Iacob et al., Nucl. Phys. A596, 155 (1996).
- [45] R. Ibbotson et al., Phys. Rev. Lett. 71, 1990 (1993).
- [46] Y. X. Luo et al., Nucl., Phys. A 818, 121 (2009).
- [47] Y. X. Luo et al., Nucl., Phys. A 838, 1 (2010).
- [48] W. R. Phillips et al., Phys. Rev. Lett. 57, 3257 (1986).
- [49] W. R. Phillips et al., Phys. Lett. B212, 402 (1988).
- [50] W. Urban et al., Phys. Lett. B185, 331 (1987).
- [51] W. Urban et al., Phys Lett B 200, 424 (1988).
- [52] W. Urban et al., Phys Lett B 258, 293 (1991).
- [53] W. Urban et al., Phys. Rev. C 54, 945 (1996).
- [54] W. Urban et al., Nucl. Phys. A613, 107 (1997).
- [55] W. Urban et al., Proceedings of the International Conference on Fission, edited by J. H. Hamilton, W. R. Phillips, and H. K. Carter (World Scientific press, Singapore, 1999), p. 136.
- [56] W. Urban et al., Acta Phys.Polon. B32, 2527 (2001).
- [57] W. Urban, et al., Phys. Rev. C 69 (2004) 017305.
- [58] S. J. Zhu et al., Phys. Lett. B357, 273 (1995).

- [59] L. Y. Zhu et al., Nucl. Phys.–Chinese Edition 22(10), 885 (1997).
- [60] S. J. Zhu et al., Phys. Rev. C 59, 1316 (1999).
- [61] S. J. Zhu et al., Phys. Rev. C 60, 051304(R) (1999).
- [62] G. Zimba et al., Phys. Rev. C 94, 054303 (2016).
- [63] R.K. Sheline and P. C. Sood, Mod. Phys. Lett. A 4, 1329 (1989).
- [64] R. A. Bark et al., Phys. Rev. Lett. 104, 022501 (2010).
- [65] T. Hayakawa et al., Eur. Phys. J. A 9, 153–156 (2000)
- [66] S. N. T. Majola, MSc thesis, University of Cape Town (2011).
- [67] S. N. T. Majola, PhD thesis, University of Cape Town (2015).
- [68] S.N.T. Majola et al., to be published in Phys. Rev. C (2019).
- [69] L. Mdletshe et al., Eur. Phys. J. A (2018) 54: 176.
- [70] G. Zimba et al., Eur. Phys. J. A (2018) 54: 59.
- [71] T. Hayakawa et al, Eur. Phys. J. A15, 299 (2002).
- [72] A Pipidis et al, Phys.Rev. C72 (2005) 064307 (2005).
- [73] <https://staff.jyu.fi/Members/ptg/folder.2006-06-01.4436246882/jurogam>
- [74] C. Rossi Alvarez, Nuclear Physics News, Volume 3, 10 (1993).
- [75] C. W. Beausang et al., Nucl.Instrum.Methods Phys.Res.A 313, 37 (1992).
- [76] G. Duchene et al., Nucl.Instrum.Methods Phys.Res. A 432, 90 (1999).
- [77] D.C. Radford. ESCL8R and LEVIT8R: Nuclear Instruments and Methods in Physics Research A, 361: 297–305 (1995).
- [78] D.C. Radford M. Cromaz and C.J. Beyer. Nuclear structure 98. AIP Conference Proceedings, Volume 481, pp. 570–580 (1999).
- [79] L.P. Ekstrom and A. Nordlund, Gamma–gamma correlations with detector arrays. Nucl, Instrum. Methods in Phys. Res, A 465:506 (1987).
- [80] A. Kramer–Flecken et al,. Use of DCO ratios for spin determination in gamma–gamma coincidence measurements, Nucl. Instrum. Methods in Phys. Res. A 275: 333 (1989).
- [81] P. A. Butler et al., Nucl. Instrum. Methods 108, 497(1973).
- [82] P. M. Jones et al., Nucl. Instr. Methods, A362, 556 (1995).
- [83] Klamra et al, Nucl., Phys. A 199, 81 (1973).
- [84] T. Grotdal et al., Mat. Fys. Medd. Dan. Vid. Selsk. 37, no 12 (1970).
- [85] <http://www.nndc.bnl.gov/chart/> (2019).

- [86] R. Bengtsson and S. Fraundorf, Nucl. Phys. A327 (1979) 139.
- [87] R. Bengtsson and S. Fraundorf, Nucl. Phys. A314 (1979) 27.
- [88] A. Celler et al., Nucl. Phys. A 432, 421 (1985).
- [89] M. Dahlinger et al., Nucl. Phys. A 484, 337 (1988).
- [90] T. Hayakawa et al., Phys. Lett B551, 79 (2003).
- [91] L. Chen et al., Phys. Rev. C 83, 034318 (2011).
- [92] S. T. Wang et al., Chin. Phys. C 33, 629 (2009).
- [93] M. A. Makhuhane, MSc thesis, University of the Western Cape (2018).
- [94] M. Sugawara et al., Nucl. Phys. A 699, 450 (2002).
- [95] L.L. Riedinger et al., Phys. Rev. Lett. 44, 568 (1980).
- [96] B.A. Alikov et al., Z. Phys. A - Atomic Nuclei 331, 265 (1988)
- [97] M.A. Riley et al., Z. Phys. A 345, 265 (1993).

Table 1: Experimentally determined properties for the nucleus ^{157}Dy . This includes excitation energy levels E_x (in keV), γ -ray energies E_γ (in keV), γ -ray intensities I_γ , assigned multiplicities (Mult), spins (for the initial and final states I_i^π and I_f^π , respectively), level in the band of destination Band#, DCO ratios (R_{DCO}) and polarization measurements (A_p). The R_{DCO} ratios were deduced by gating on stretched E2 transitions with the exception of those marked by an asterisk, which were deduced by gating on a pure stretched dipole. Quantities within parenthesis are quoted as tentative while empty entries refer to information that could not be obtained.

$E_x(\text{keV})$	$E_\gamma(\text{keV})^l$	I_γ	Mult	I_i^π	I_f^π	Band#	R_{DCO}	A_p
Band1								
61	61.0	21.6(16)	M1/E2	5/2 ⁻	3/2 ⁻	Band2		
257	109.9	18.7(6)	M1/E2	9/2 ⁻	7/2 ⁻	Band2		
257	196.4	19.8(7)	E2	9/2 ⁻	5/2 ⁻	Band1		0.13(3)
548	147.1	9.3(3)	M1/E2	13/2 ⁻	11/2 ⁻	Band2		
548	290.6	22.7(7)	E2	13/2 ⁻	9/2 ⁻	Band1	0.85(16)	0.07(1)
920	171.0	2.25(7)	M1/E2	17/2 ⁻	15/2 ⁻	Band2		
920	372.3	14.1(4)	E2	17/2 ⁻	13/2 ⁻	Band1	0.99(10)	0.09(2)
1358	184.5	0.85(3)	M1/E2	21/2 ⁻	19/2 ⁻	Band2		
1358	438.2	6.42(19)	E2	21/2 ⁻	17/2 ⁻	Band1	1.04(12)	0.08(2)
1849	490.7	2.31(7)	E2	25/2 ⁻	21/2 ⁻	Band1	1.11(30)	
2381	532.2	0.57(2)	E2	29/2 ⁻	25/2 ⁻	Band1	1.40(49)	
Band2								
147	86.5	44.7(14)	M1/E2	7/2 ⁻	5/2 ⁻	Band1		
147	147.5	15.6(6)	E2	7/2 ⁻	3/2 ⁻	Band2		
401	143.6	14.8(5)	M1/E2	11/2 ⁻	9/2 ⁻	Band1		
401	253.4	20.1(6)	E2	11/2 ⁻	7/2 ⁻	Band2		
749	201.2	5.51(17)	M1/E2	15/2 ⁻	13/2 ⁻	Band1		-0.08(8)
749	348.3	15.8(5)	E2	15/2 ⁻	11/2 ⁻	Band2	0.89(16)	0.09(2)
1174	253.5	1.69(6)	M1/E2	19/2 ⁻	17/2 ⁻	Band1		-0.08(2)
1174	424.5	7.37(22)	E2	19/2 ⁻	15/2 ⁻	Band2	0.93(16)	0.11(3)
1655	296.5	0.61(3)	M1/E2	23/2 ⁻	21/2 ⁻	Band1		
1655	481.3	2.96(9)	E2	23/2 ⁻	19/2 ⁻	Band2	0.99(17)	0.09(3)
2177	522.2	0.89(3)	E2	27/2 ⁻	23/2 ⁻	Band2	0.91(17)	0.09(5)
2735	557.6	0.20(1)	E2	31/2 ⁻	27/2 ⁻	Band2	1.03(6)	
Band3								
238	76.5	≈100	E2	13/2 ⁺	9/2 ⁺	Band3		
435	196.9	98(3)	E2	17/2 ⁺	13/2 ⁺	Band3		0.13(3)
746	311.0	52.1(16)	E2	21/2 ⁺	17/2 ⁺	Band3	0.83(8)	0.10(2)

$E_x(\text{keV})$	$E_\gamma(\text{keV})^l$	I_γ	<i>Mult</i>	I_i^π	I_f^π	<i>Band#</i>	<i>Rdco</i>	A_p
Band3 continued								
1157	410.8	16.6(5)	E2	25/2 ⁺	21/2 ⁺	Band3	0.92(10)	0.08(2)
1652	495.1	4.10(13)	E2	29/2 ⁺	25/2 ⁺	Band3	1.19(16)	0.06(2)
2218	566.4	0.89(3)	E2	33/2 ⁺	29/2 ⁺	Band3	0.86(16)	0.04(5)
2844	625.5	0.25(1)	E2	37/2 ⁺	33/2 ⁺	Band3		
Band 3_L								
188	127.2	0.05(2)	E1	5/2 ⁺	5/2 ⁻	Band1		
188	188.2	0.5(2)	E1	5/2 ⁺	3/2 ⁻	Band2		0.38(15)
Band4								
211	150.0	3.35(10)	E1	7/2 ⁺	5/2 ⁻	Band1		
298	86.8	7.16(10)	E2	11/2 ⁺	7/2 ⁺	Band4		
298	136.2	1.58(16)	M1/E2	11/2 ⁺	9/2 ⁺	Band3		
512	76.5	5.65(20)	M1/E2	15/2 ⁺	17/2 ⁺	Band3		
512	213.7	16.9(6)	E2	15/2 ⁺	11/2 ⁺	Band4		0.11(3)
512	273.5	10.2(4)	M1/E2	15/2 ⁺	13/2 ⁺	Band3	0.66(8)	-0.03(2)
844	97.8	2.58(8)	M1/E2	19/2 ⁺	21/2 ⁺	Band3		
844	332.4	24.0(7)	E2	19/2 ⁺	15/2 ⁺	Band4	0.89(8)	0.09(2)
844	408.8	9.1(3)	M1/E2	19/2 ⁺	17/2 ⁺	Band3		
1281	123.5	0.70(3)	M1/E2	23/2 ⁺	25/2 ⁺	Band3		
1281	436.7	11.4(3)	E2	23/2 ⁺	19/2 ⁺	Band4	1.12(10)	0.08(1)
1281	534.5	1.70(6)	M1/E2	23/2 ⁺	21/2 ⁺	Band3		
1807	154.9	0.18(2)	M1/E2	27/2 ⁺	29/2 ⁺	Band3		
1807	526.5	3.04(9)	E2	27/2 ⁺	23/2 ⁺	Band4	1.12(8)	0.71(4)
1807	649.9	0.52(3)	M1/E2	27/2 ⁺	25/2 ⁺	Band3		
2410	603.2	0.84(4)	E2	31/2 ⁺	27/2 ⁺	Band4		
Bands								
341	106.5	0.13(3)	E1	5/2 ⁻	3/2 ⁺	Band7		
341	152.8	0.17(2)	E1	5/2 ⁻	5/2 ⁺	Band 3_L		
341	280.0	0.61(6)	M1/E2	5/2 ⁻	5/2 ⁻	Band1	0.71(7)	
341	341.0	0.41(5)	M1/E2	5/2 ⁻	3/2 ⁻	Band2		
527	91.5	0.29(3)	E1	9/2 ⁻	7/2 ⁺	Band7		
527	106.6	0.47(4)	M1/E2	9/2 ⁻	7/2 ⁻	Band6		
527	125.7	1.12(5)	M1/E2	9/2 ⁻	11/2 ⁻	Band2		
527	185.6	0.99(5)	E2	9/2 ⁻	5/2 ⁻	Band5		
527	228.8	1.20(8)	E1	9/2 ⁻	11/2 ⁺	Band4	0.52(31)	0.03(2)
527	269.5	2.21(10)	M1/E2	9/2 ⁻	9/2 ⁻	Band1	0.87(22)	-0.27(11)
527	365.0	0.83(6)	E1	9/2 ⁻	9/2 ⁺	Band3	1.12(4)	-0.07(2)
527	379.5	0.81(5)	M1/E2	9/2 ⁻	7/2 ⁻	Band2	0.61(7)	
527	465.7	1.34(7)	E2	9/2 ⁻	5/2 ⁻	Band1	1.23(3)	

$E_x(\text{keV})$	$E_\gamma(\text{keV})^I$	I_γ	<i>Mult</i>	I_i^π	I_f^π	<i>Band#</i>	R_{DCO}	A_p
<i>Band5 continued</i>								
827	140.5	0.56(3)	E1	13/2 ⁻	11/2 ⁺	Band7		
827	154.9	0.55(4)	M1/E2	13/2 ⁻	11/2 ⁻	Band6		
827	278.5	0.68(4)	M1/E2	13/2 ⁻	13/2 ⁻	Band1		
827	299.9	3.93(13)	E2	13/2 ⁻	9/2 ⁻	Band5	0.83(23)	0.09(4)
827	314.9	0.63(2)	E1	13/2 ⁻	15/2 ⁺	Band4	0.42(18)	
827	425.6	2.15(8)	M1/E2	13/2 ⁻	11/2 ⁻	Band2	0.47(27)	-0.02(2)
827	569.5	2.30(9)	E2	13/2 ⁻	9/2 ⁻	Band1	1.11(6)	0.07(7)
1214	294.3	0.031(2)	M1/E2	17/2 ⁻	17/2 ⁻	Band1		
1214	388.0	3.19(10)	E2	17/2 ⁻	13/2 ⁻	Band5	1.15(3)	0.11(2)
1214	465.3	0.90(3)	M1/E2	17/2 ⁻	15/2 ⁻	Band1		
1214	666.5	0.52(3)	E2	17/2 ⁻	13/2 ⁻	Band1		
1214	779.3	0.64(4)	E1	17/2 ⁻	17/2 ⁺	Band3		
1665	450.2	1.50(5)	E2	21/2 ⁻	17/2 ⁻	Band5	1.23(28)	0.04(2)
1665	491.1	0.17(2)	M1/E2	21/2 ⁻	19/2 ⁻	Band2	0.93(3)	0.07(2)
2154	489.5	0.35(2)	E2	25/2 ⁻	21/2 ⁻	Band5		
<i>Band6</i>								
420	162.7	2.10(11)	M1/E2	7/2 ⁻	9/2 ⁻	Band1	0.54(17)	
420	209.0	2.00(19)	E1	7/2 ⁻	7/2 ⁺	Band4	0.95(8)	
420	258.4	2.16(18)	E1	7/2 ⁻	9/2 ⁺	Band3		
420	272.5	4.81(22)	M1/E2	7/2 ⁻	7/2 ⁻	Band2		
420	359.1	0.72(11)	M1/E2	7/2 ⁻	5/2 ⁻	Band1		
420	420.0	1.02(13)	E2	7/2 ⁻	3/2 ⁻	Band2	2.19(10)*	
672	123.6	0.40(3)	M1/E2	11/2 ⁻	13/2 ⁻	Band1		
672	251.6	1.41(7)	E2	11/2 ⁻	7/2 ⁻	Band6		
672	270.7	1.13(6)	M1/E2	11/2 ⁻	11/2 ⁻	Band2		
672	373.8	1.12(9)	E1	11/2 ⁻	11/2 ⁺	Band4		
672	414.5	1.28(7)	M1/E2	11/2 ⁻	9/2 ⁻	Band1		
672	433.3	2.63(12)	E1	11/2 ⁻	13/2 ⁺	Band3		0.12(1)
672	510.0	4.4(3)	E1	11/2 ⁻	9/2 ⁺	Band3		
672	524.5	0.76(6)	E2	11/2 ⁻	7/2 ⁻	Band2		
1021	272.1	0.61(4)	M1/E2	15/2 ⁻	15/2 ⁻	Band2		
1021	349.7	2.58(9)	E2	15/2 ⁻	11/2 ⁻	Band6		0.23(8)
1021	473.3	0.59(3)	M1/E2	15/2 ⁻	13/2 ⁻	Band1		
1021	586.1	1.56(7)	E1	15/2 ⁻	17/2 ⁺	Band3	0.54(31)	0.07(2)
1021	620.4	0.77(4)	E2	15/2 ⁻	11/2 ⁻	Band2		
1021	783.0	2.18(10)	E1	15/2 ⁻	13/2 ⁺	Band3	0.74(27)	0.12(8)
1441	419.6	1.43(5)	E2	19/2 ⁻	15/2 ⁻	Band6	2.20(11)*	0.07(1)

$E_x(\text{keV})$	$E_\gamma(\text{keV})^l$	I_γ	<i>Mult</i>	I_i^π	I_f^π	<i>Band#</i>	<i>R_{DCO}</i>	A_p
<i>Band6 continued</i>								
1441	694.7	2.32(8)	E1	19/2 ⁻	21/2 ⁺	Band3		
1441	1005.7	3.23(11)	E1	19/2 ⁻	17/2 ⁺	Band3		0.04(2)
1905	463.9	0.52(2)	E2	23/2 ⁻	19/2 ⁻	Band6	0.89(4)	0.18(8)
1905	747.8	0.55(2)	E1	23/2 ⁻	25/2 ⁺	Band3		
1905	1158.9	1.48(5)	E1	23/2 ⁻	21/2 ⁺	Band3		0.11(6)
2413	507.8	0.83(3)	E2	27/2 ⁻	23/2 ⁻	Band6		
2413	1255.6	0.61(2)	E1	27/2 ⁻	25/2 ⁺	Band3		
<i>Band7</i>								
235	234.6	2.6(4)	E1	3/2 ⁺	3/2 ⁻	Band2		-0.18(2)
235	173.6	2.0(3)	E1	3/2 ⁺	5/2 ⁻	Band1		
435	83.3	0.37(3)	M1/E2	7/2 ⁺	(5/2 ⁺)	Band8		
435	94.4	0.12(3)	E1	7/2 ⁺	5/2 ⁻	Band5		
435	200.8	0.91(5)	E2	7/2 ⁺	3/2 ⁺	Band8		0.06(1)
435	224.4	3.19(23)	M1/E2	7/2 ⁺	7/2 ⁺	Band4	0.80(18)	
435	273.7	2.12(17)	M1/E2	7/2 ⁺	9/2 ⁺	Band3		
686	118.5	0.34(3)	M1/E2	11/2 ⁺	9/2 ⁺	Band10		
686	159.5	0.46(4)	E1	11/2 ⁺	9/2 ⁻	Band5		
686	251.0	3.13(11)	E2	11/2 ⁺	7/2 ⁺	Band7		
686	388.3	0.97(6)	M1/E2	11/2 ⁺	11/2 ⁺	Band4		0.09(7)
686	448.0	1.84(9)	M1/E2	11/2 ⁺	13/2 ⁺	Band3		
686	524.5	0.41(6)	M1/E2	11/2 ⁺	9/2 ⁺	Band3		
1025	149.4	0.55(3)	M1/E2	15/2 ⁺	13/2 ⁺	Band8		
1025	339.0	1.98(7)	E2	15/2 ⁺	11/2 ⁺	Band7	1.12(19)	0.17(2)
1025	513.4	0.47(16)	M1/E2	15/2 ⁺	15/2 ⁺	Band4		
1025	590.1	1.39(6)	M1/E2	15/2 ⁺	17/2 ⁺	Band3		
1025	787.0	2.89(12)	M1/E2	15/2 ⁺	13/2 ⁺	Band3		-0.04(1)
1421	395.8	1.83(6)	E2	19/2 ⁺	15/2 ⁺	Band7	0.95(6)	0.06(6)
1421	577.5	1.14(5)	M1/E2	19/2 ⁺	19/2 ⁺	Band4	0.68(31)	
1421	674.9	0.53(3)	M1/E2	19/2 ⁺	21/2 ⁺	Band3	0.61(25)	
1421	985.9	1.39(6)	M1/E2	19/2 ⁺	17/2 ⁺	Band3		
1897	475.5	1.25(5)	E2	23/2 ⁺	19/2 ⁺	Band7		0.28(8)
1897	739.5	0.48(2)	M1/E2	23/2 ⁺	25/2 ⁺	Band3		
1897	1150.6	0.55(3)	M1/E2	23/2 ⁺	21/2 ⁺	Band3		
2393	496.2	0.64(3)	E2	(27/2 ⁺)	23/2 ⁺	Band7	0.883(103)	
<i>Band8</i>								
352	117.4	0.19(3)	M1/E2	(5/2 ⁺)	3/2 ⁺	Band7		
352	163.9	2.41(8)	M1/E2	(5/2 ⁺)	5/2 ⁺	Band 3_L		0.04(1)
568	132.0	0.35(3)	M1/E2	9/2 ⁺	7/2 ⁺	Band7		

$E_x(\text{keV})$	$E_\gamma(\text{keV})^{\dagger}$	I_γ	<i>Mult</i>	I_i^π	I_f^π	<i>Band#</i>	R_{DCO}	A_p
<i>Band8 continued</i>								
568	147.6	1.48(8)	E1	9/2 ⁺	7/2 ⁻	Band6		
568	215.6	2.01(8)	E2	9/2 ⁺	(5/2 ⁺)	Band8		
568	356.6	0.48(6)	M1/E2	9/2 ⁺	7/2 ⁺	Band4		
568	380.0	0.40(3)	E2	9/2 ⁺	5/2 ⁺	Band 3_L	2.49(15)*	0.11(2)
568	405.9	5.08(24)	M1/E2	9/2 ⁺	9/2 ⁺	Band3		
876	203.9	0.76(5)	E1	13/2 ⁺	11/2 ⁻	Band6		
876	307.8	4.0(1)	E2	13/2 ⁺	9/2 ⁺	Band8		0.06(6)
876	577.7	1.02(8)	M1/E2	13/2 ⁺	11/2 ⁺	Band4		
876	637.5	2.31(11)	M1/E2	13/2 ⁺	13/2 ⁺	Band3		0.09(7)
876	713.9	1.58(16)	E2	13/2 ⁺	9/2 ⁺	Band3		
1248	372.0	2.61(9)	E2	17/2 ⁺	13/2 ⁺	Band8		
1248	498.6	0.46(3)	E1	17/2 ⁺	15/2 ⁻	Band2		
1248	736.4	2.23(9)	M1/E2	17/2 ⁺	15/2 ⁺	Band4		
1248	812.5	1.95(9)	M1/E2	17/2 ⁺	17/2 ⁺	Band3		
1248	1009.5	1.58(16)	E2	17/2 ⁺	13/2 ⁺	Band3		
1732	451.5	0.45(2)	M1/E2	(21/2 ⁺)	23/2 ⁺	Band4		
1732	484.5	0.75(3)	E2	(21/2 ⁺)	17/2 ⁺	Band8		0.06(9)
1732	888.2	0.91(4)	M1/E2	(21/2 ⁺)	19/2 ⁺	Band4		
1732	986.2	1.54(20)	M1/E2	(21/2 ⁺)	21/2 ⁺	Band3		
2212	480.1	0.49(3)	E2	(25/2 ⁺)	21/2 ⁺	Band8		

[†]Typical uncertainty of 0.3 keV and up to 0.5 keV for weak transitions ($I_\gamma < 1$).